

Seismic Invisibility: Elastic wave cloaking via symmetrized transformation media

Sophia R. Sklan,¹ Ronald Y.S. Pak,² and Baowen Li¹

¹*Department of Mechanical Engineering, University of Colorado Boulder, Colorado 80309 USA*

²*Department of Civil Engineering, University of Colorado Boulder, Colorado 80309 USA*

Transformation media theory, which steers waves in solids via an effective geometry induced by a refractive material (Fermat's principle of least action), provides a means of controlling vibrations and elastic waves beyond the traditional dissipative structures regime. In particular, it could be used to create an elastic wave cloak, shielding an interior region against elastic waves while simultaneously preventing scattering in the outside domain. However, as a true elastic wave cloak would generally require materials with stiffness tensors lacking the minor symmetry (implying asymmetric stress), the utility of such an elastic wave cloak has thus far been limited by the challenge of fabricating these materials. Here we develop a means of overcoming this limitation via the development of a symmetrized elastic cloak, sacrificing some of the performance of the perfect cloak for the sake of restoring the minor symmetry. We test the performance of the symmetrized elastic cloak for shielding a tunnel against seismic waves, showing that it can be used to reduce the average displacement within the tunnel by an order of magnitude (and reduce energy by two orders of magnitude) for waves above a critical frequency of the cloak. This critical frequency, which corresponds to the generation of surface waves at the cloak-interior interface, can be used to develop a simple heuristic model of the symmetrized elastic cloak's performance for a generic problem.

The need to protect objects against unwanted mechanical vibration and wave incidence is a long-standing subject in engineering [1, 2]. The problem arises in multiple scenarios including blocking sound/elastic waves and eliminating unwanted mechanical resonances [1, 2] (vibration isolation) or guarding against nonlinear mechanical shock waves and preventing the collapse of structures under incident seismic waves [3, 4] (earthquake engineering). Techniques to accomplish these goals have included strengthening structures, modifying structural resonances through additive engineering or anti-resonance, developing flexible structures that can withstand large deformations, or including dissipative elements [1–4]. Recently, techniques from phononics and acoustic wave engineering have been adapted to vibration isolation/earthquake engineering (VIEE), most prominently by the inclusion of phononic/sonic crystals as a means of shielding against seismic surface waves [1, 4–11] (which contain a much smaller portion of energy from an earthquake than bulk waves, particularly shear waves [12]). However, one limitation of all these techniques is that they can only seek to mitigate elastic waves, reducing the local amplitude of the earthquake or allowing a structure to withstand an unmodified vibration. In addition, many of these techniques have focused upon narrow frequency bands (e.g. modifying resonances), particularly for low frequency applications. While these are primary concerns, minimization of broadband or higher frequency transmissions to a structure is of increasing engineering interest nowadays as the reliance on electronic-computer control of critical equipment grows.

An alternative framework to VIEE would be cloaking. Cloaks modify the environment around a region such that waves are refracted around a central domain [13–18]. Since the energy is redirected, not dissipated, it could in principle be used to control vibrations of arbitrary amplitude or frequency (in practice, engineering limitations prevent perfect performance). Developing effective, realizable cloaks is an

active field of research in optics and acoustics, but application to elastic waves and VIEE has remained in its infancy [19–25]. The central challenge limiting the utilization of cloaking for these applications is that transformation media theory, the mathematical framework underlying the operation of the cloak, is not feasible for a generic elastic wave. As was shown by Milton et al., a cloaking transformation for an elastic wave would break the stiffness tensor's minor symmetry ($c_{ijkl} = c_{jikl} = c_{ijlk}$) [26]. Since this symmetry exists for all commonplace solid materials, this has limited elastic wave cloaks to special cases where the loss of minor symmetry is irrelevant (e.g. planar structures, partial coordinate transformations) or structures with significant fabrication challenges (e.g. Cosserat materials and auxetic/pentamode materials, hyperelastic metamaterials, Willis materials) [27–37]. Hyperelastic metamaterials [38] deserve special mention as a system where the nonlinear pre-stress of the system does allow for the more ready construction of materials lacking minor elastic symmetry. However, fabrication challenges and the need for strong nonlinearity still limit the widespread application of the technique. Similarly, Willis materials [26] provide an explicit solution where the loss of minor symmetry is preserved, but at the cost of introducing highly dispersive materials which distort the waves and thus limit the utility of broadband cloaking. Moreover, the incorporation of Willis materials at a theoretical level has not noticeably reduced the fabrication challenges of constructing an elastic wave cloak.

In this work we present a framework for an approximate elastic cloak, which preserves minor symmetries even in the most general case. This symmetrized elastic cloak (SEC) has the advantage of being, in principle, more readily realizable, but comes at the cost of no longer being a perfect cloak. However, a cloak generally performs two tasks: preventing scattering of an incoming wave as it propagates around and through the cloak (stealth, the primary concern in optical or acoustic cloaking) and blocking waves from penetrating a central

region (shielding, the primary concern in VIEE). The performance of an approximate cloak for both these tasks is an open question, but only the latter performance metric is important for VIEE applications. As such, we characterize the performance of the cloak in the simplest physically realistic scenario – shielding a tunnel or a round shell buried in a soil-type medium from seismic waves. Through this analysis, we derive the limitations of the SEC and present a simple holistic model that captures the essential performance characteristics.

To begin, the equations of motion in Cartesian coordinates for elastic waves in a solid are

$$\rho \partial_{tt} u_i = \partial_j \sigma_{ji} \quad (1)$$

$$\sigma_{ij} = c_{ijkl} \epsilon_{kl} \quad (2)$$

$$\epsilon_{ij} = \frac{1}{2} (\partial_j u_i + \partial_i u_j), \quad (3)$$

(where ρ is density, u is the displacement vector, ϵ is the infinitesimal strain tensor, σ is the Cauchy stress tensor, and c is the 4th order stiffness tensor). In cylindrical coordinates they become

$$\begin{aligned} \rho \partial_{tt} u_r &= \frac{1}{r} \partial_r r \sigma_{rr} + \frac{1}{r} (\partial_\theta \sigma_{\theta r} - \sigma_{\theta\theta}) + \partial_z \sigma_{zr} \\ \rho \partial_{tt} u_\theta &= \frac{1}{r} \partial_r r \sigma_{r\theta} + \frac{1}{r} (\partial_\theta \sigma_{\theta\theta} + \sigma_{\theta r}) + \partial_z \sigma_{z\theta} \\ \rho \partial_{tt} u_z &= \frac{1}{r} \partial_r r \sigma_{rz} + \frac{1}{r} \partial_\theta \sigma_{\theta z} + \partial_z \sigma_{zz}, \end{aligned} \quad (4)$$

while $\sigma_{ij} = c_{ijkl} \epsilon_{ij}$ is unchanged except for a relabeling of coordinates, and

$$\bar{\epsilon} = \begin{bmatrix} \partial_r u_r \hat{e}_r \hat{e}_r & \frac{1}{r} (\partial_\theta u_r - u_\theta) \hat{e}_r \hat{e}_\theta & \partial_z u_r \hat{e}_r \hat{e}_z \\ \partial_r u_\theta \hat{e}_\theta \hat{e}_r & \frac{1}{r} (\partial_\theta u_\theta + u_r) \hat{e}_\theta \hat{e}_\theta & \partial_z u_\theta \hat{e}_\theta \hat{e}_z \\ \partial_r u_z \hat{e}_z \hat{e}_r & \frac{1}{r} \partial_\theta u_z \hat{e}_z \hat{e}_\theta & \partial_z u_z \hat{e}_z \hat{e}_z \end{bmatrix} \quad (5)$$

where we've dropped the explicit symmetry of ϵ and σ by requiring it be preserved in c . In general, c must possess both the major symmetry

$$c_{ijkl} = c_{klij} \quad (6)$$

(which comes from the symmetry of mixed partials) and the minor symmetry

$$c_{ijkl} = c_{jikl} = c_{ijlk} = c_{jilk} \quad (7)$$

(which comes from the physical symmetry of stress and strain). The standard cylindrical cloaking transformation [13] is the dilation

$$r' = \frac{b-a}{b} r + a \quad (8)$$

where r' is the transformed radial coordinate, a is the inner radius of the cloak, and b is the outer radius of the cloak. Under the cloaking transformation, we seek a set of c' and ρ' such that the equation of motion in the standard frame (i.e. equation (4)) with these materials is the same as the equation of motion in the transformed frame (equation (4) with all factors of r replaced by r' but $\bar{u}' = \bar{u}$ and $\sigma' \neq \sigma$) with some trivial background material. Breaking the minor symmetry, this can be accomplished exactly using a density and stiffness tensor

$$\rho' = \rho_0 \frac{r-a}{r} \left(\frac{b}{b-a} \right)^2 \quad (9)$$

$$c'_{ijkl} = \begin{pmatrix} \frac{r-a}{r} & & & \\ & 1 & & \\ & & \frac{b}{b-a} \frac{r-a}{r} & \\ & & & \end{pmatrix} \times \begin{pmatrix} \begin{bmatrix} C_{rrrr} & C_{rrr\theta} & C_{rrrz} \\ \frac{r}{r-a} C_{rrr\theta} & \frac{r}{r-a} C_{rr\theta\theta} & \frac{r}{r-a} C_{rr\theta z} \\ \frac{b}{b-a} C_{rrzr} & \frac{b}{b-a} C_{rrz\theta} & \frac{b}{b-a} C_{rrzz} \end{bmatrix} & \begin{bmatrix} C_{r\theta rr} & C_{r\theta r\theta} & C_{r\theta rz} \\ \frac{r}{r-a} C_{r\theta\theta r} & \frac{r}{r-a} C_{r\theta\theta\theta} & \frac{r}{r-a} C_{r\theta\theta z} \\ \frac{b}{b-a} C_{r\theta zr} & \frac{b}{b-a} C_{r\theta z\theta} & \frac{b}{b-a} C_{r\theta zz} \end{bmatrix} & \begin{bmatrix} C_{rzrr} & C_{rzr\theta} & C_{rzrz} \\ \frac{r}{r-a} C_{rzr\theta} & \frac{r}{r-a} C_{rz\theta\theta} & \frac{r}{r-a} C_{rz\theta z} \\ \frac{b}{b-a} C_{rz zr} & \frac{b}{b-a} C_{rz z\theta} & \frac{b}{b-a} C_{rz zz} \end{bmatrix} \\ \begin{bmatrix} C_{\theta rrr} & C_{\theta r r\theta} & C_{\theta r rz} \\ \frac{r}{r-a} C_{\theta r\theta r} & \frac{r}{r-a} C_{\theta r\theta\theta} & \frac{r}{r-a} C_{\theta r\theta z} \\ \frac{b}{b-a} C_{\theta r zr} & \frac{b}{b-a} C_{\theta r z\theta} & \frac{b}{b-a} C_{\theta r zz} \end{bmatrix} & \begin{bmatrix} C_{\theta\theta rr} & C_{\theta\theta r\theta} & C_{\theta\theta rz} \\ \frac{r}{r-a} C_{\theta\theta\theta r} & \frac{r}{r-a} C_{\theta\theta\theta\theta} & \frac{r}{r-a} C_{\theta\theta\theta z} \\ \frac{b}{b-a} C_{\theta\theta zr} & \frac{b}{b-a} C_{\theta\theta z\theta} & \frac{b}{b-a} C_{\theta\theta zz} \end{bmatrix} & \begin{bmatrix} C_{\theta zrr} & C_{\theta zr\theta} & C_{\theta zrz} \\ \frac{r}{r-a} C_{\theta z\theta r} & \frac{r}{r-a} C_{\theta z\theta\theta} & \frac{r}{r-a} C_{\theta z\theta z} \\ \frac{b}{b-a} C_{\theta z zr} & \frac{b}{b-a} C_{\theta z z\theta} & \frac{b}{b-a} C_{\theta z zz} \end{bmatrix} \\ \begin{bmatrix} C_{zrrr} & C_{zrr\theta} & C_{zrrz} \\ \frac{r}{r-a} C_{zr\theta r} & \frac{r}{r-a} C_{zr\theta\theta} & \frac{r}{r-a} C_{zr\theta z} \\ \frac{b}{b-a} C_{zr zr} & \frac{b}{b-a} C_{zr z\theta} & \frac{b}{b-a} C_{zr zz} \end{bmatrix} & \begin{bmatrix} C_{z\theta rr} & C_{z\theta r\theta} & C_{z\theta rz} \\ \frac{r}{r-a} C_{z\theta\theta r} & \frac{r}{r-a} C_{z\theta\theta\theta} & \frac{r}{r-a} C_{z\theta\theta z} \\ \frac{b}{b-a} C_{z\theta zr} & \frac{b}{b-a} C_{z\theta z\theta} & \frac{b}{b-a} C_{z\theta zz} \end{bmatrix} & \begin{bmatrix} C_{zzrr} & C_{zzr\theta} & C_{zzrz} \\ \frac{r}{r-a} C_{zz\theta r} & \frac{r}{r-a} C_{zz\theta\theta} & \frac{r}{r-a} C_{zz\theta z} \\ \frac{b}{b-a} C_{zz zr} & \frac{b}{b-a} C_{zz z\theta} & \frac{b}{b-a} C_{zz zz} \end{bmatrix} \end{pmatrix}. \quad (10)$$

Note that this preserves major symmetry of c and that the transformation of c_{ijkl} is effectively independent of two indices (either i or j and either k or l).

Because equation (10) has lost minor symmetry, however,

it is no longer easily realizable. To restore this symmetry, we impose a symmetrization function

$$c_{ijkl}^S = S(c_{ijkl}, c_{jikl}, c_{ijlk}, c_{jilk}) \quad (11)$$

where S is an arbitrary function that preserves minor symme-

constrained by the feature size of the metamaterials used in its fabrication). This tunnel was placed in the center of a rectangular domain (100m×300m) of soil. For boundary conditions, the top surface was left traction-free ($\sigma \cdot \hat{n} = 0$), with the sides left as impedance matched absorbing layers. (Note that a true impedance matching requires breaking the minor symmetry [39]. Instead, we only use the pre-defined “low reflecting boundary” setting of COMSOL [41], which imposes a boundary that only approximately impedance matches every polarization and will introduce some amount of reflection. The simulation domain’s boundaries were set to minimize the impact of these reflections on the performance of the SEC.) From the base, a vibration of $u_i = u_{i0} \sin(2\pi\omega t)\hat{e}_i$ was imposed, with $u_{i0} = 1\text{cm}$ and $i = x, y$ for S or P waves respectively. Frequencies of the imposed waves were allowed to vary between 1 and 10 Hz, as those are the most relevant frequencies for typical earthquakes [42]. In addition, a second set of boundary conditions are considered where waves approach parallel to the surface, i.e. the displacement is imposed upon one of the sides and the base is left impedance matched. This second set of boundary conditions was used to account for any effects induced by the anisotropy of the boundary conditions; the operation of the cloak in infinite homogeneous space is expected to retain isotropy. To measure the efficiency of the cloak, we employ two metrics: reduction in average energy and reduction in average displacement. These are characterized as efficiencies,

$$\eta(E) = 1 - \langle E \rangle_C / \langle E \rangle_U \quad (15)$$

and

$$\eta(u_i) = 1 - \langle |u_i| \rangle_C / \langle |u_i| \rangle_U \quad (16)$$

where brackets denote averaging over the concrete shell and averaging over time, E is total energy, U refers to results with no cloak, and C refers to results with the cloak. Given that we consider two directions of incident waves (other directions can be decomposed into a linear superposition of these orthogonal cases), we define u_{\parallel} as the response with polarization parallel to the driving force and u_{\perp} as the transverse response (in general $u_{\parallel} \gg u_{\perp}$, $\eta(u_{\perp})$, $\eta(v_i)$, $\eta(a_i)$ in supplement). Note that $\eta \leq 1$ for a passive cloak, with $\eta = 1$ being perfect cloaking (100% efficiency), $\eta = 0$ being no improvement, and $\eta < 0$ being a degradation of performance due to the cloak. With this setup, we use COMSOL [41] to simulate the tunnel with and without the cloak for varying boundary conditions ($\vec{u} = 0$ initial conditions, simulation interval of $180/\omega$). Simulations used a mesh grid of 9924 domain elements and 388 boundary elements (i.e. an “extremely fine mesh” setting), which showed a strong convergence and included a time resolution of $1/20\omega$. Numerical integration was performed using the pre-built COMSOL finite element differential equation solver using MUMPS at COMSOL’s default settings and displacements explicitly constrained to real values.

Examining the performance of the SEC under this efficiency metric, we can separate out two different regimes for

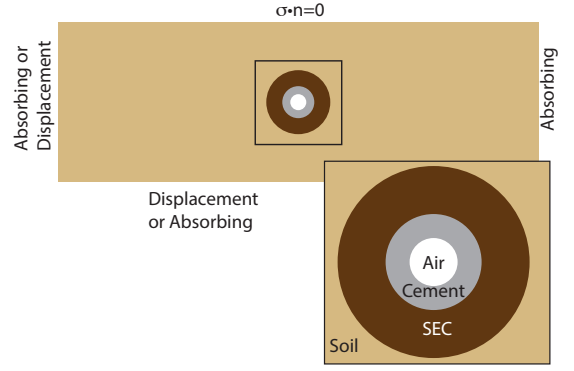


FIG. 1: Schematic model of SEC tunnel shield simulation setup. The cloak and tunnel are placed at the center of simulation domain, with boundary conditions labeled at each end. (Inset) Material structure of the simulation: Soil (light brown) surrounds the SEC (dark brown ring). Inside the SEC is a concrete (grey ring) wall filled with air (white circle).

each polarization. For S waves (see Figure 2A-B), the performance is relatively insensitive to the direction of the incident waves, but shows a clear change in performance above and below approximately $1\text{Hz} \equiv \omega_{c,S}$. For $\omega \lesssim 1\text{Hz}$, the SEC clearly reduces the performance of the concrete in blocking incoming waves, reaching its minimum performance at $\omega \approx 1\text{Hz}$ ($\eta(u_{\parallel,S}) \gtrsim -2.00$, $\eta(E_S) \gtrsim -8.11$).

On the other hand, for $\omega \gtrsim 1\text{Hz}$ the SEC shows great improvement in performance; the concrete shell is protected from incoming waves by an order of magnitude for displacement and two orders of magnitude for energy ($\eta(u_{\parallel,S}) \lesssim 0.849$, $\eta(E_S) \lesssim 0.988$). P waves (see Figure 2C-D) are similar to S waves but the critical frequency separating these regimes is shifted to $2\text{Hz} \equiv \omega_{c,P}$ ($\eta(u_{\parallel,P}) \lesssim 0.913$, $\eta(E_P) \lesssim 0.993$) due to the difference in speeds $v_P/v_S = \sqrt{6} \approx 2.4$ (where v_i is the velocity, $\sqrt{\mu/\rho}$ for S waves and $\sqrt{(\lambda + 2\mu)/\rho}$ for P waves). Note that, for ω under the critical frequency, some of the simulations demonstrated small oscillations between positive and negative efficiency. However, as simulations far below the critical frequency possess wavelengths on the order of kilometers or longer, and the cloak is on the order of meters, we expect that these effects are highly sensitive to boundary conditions and may be numerical artifacts.

To explain the difference in performance above and below these critical frequencies, we examine the energy difference between the cloaked and uncloaked cases as a function of time for different incident frequencies (see Figure 3). Below the critical frequency (Figure 3A), we see a very clear buildup of energy near the inner surface of the cloak. While such an energy buildup exists for frequencies above the critical frequency (Figure 3B), it remains relatively localized in those cases. At or below the critical frequency, though, the surface energy concentration extends across nearly the entire length of the inner boundary, meaning that an effectively uniform

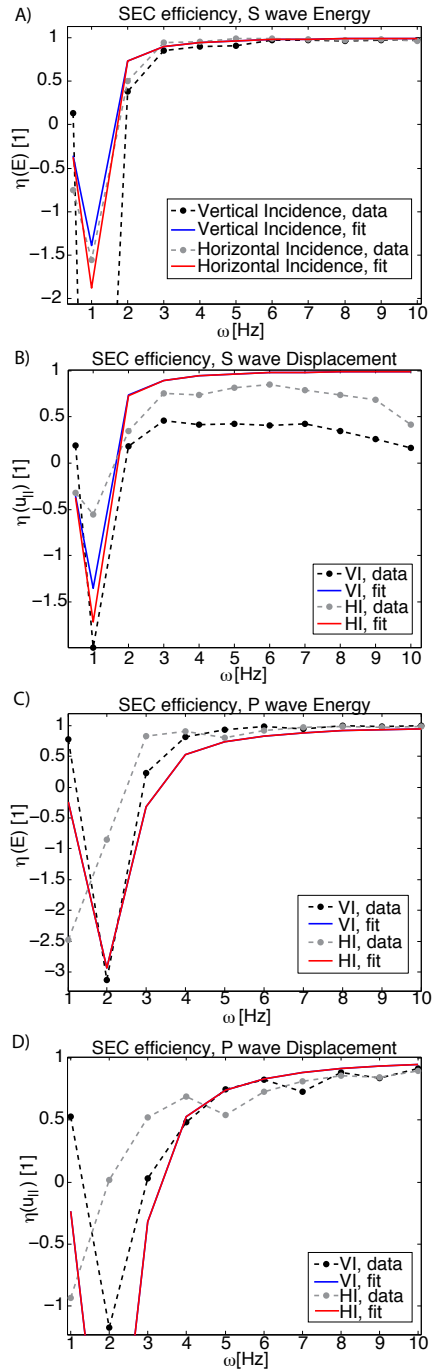


FIG. 2: Efficiency plots for the SEC as a function of frequency. Black dashed curve is data for vertical incidence (VI, wave from beneath the SEC), grey dashed curve is data for horizontal incidence (HI, wave from the left side of the SEC), while solid blue and red curves are fitted harmonic oscillator models of the SEC for VI and HI respectively. Fits are generated by matching the data generated through direct COMSOL simulations of the dynamics with a simple harmonic oscillator model given in equation (18). (A) Energy efficiency, S wave. Efficiency at the cutoff frequency of 1Hz (value given in main text) cropped to distinguish higher frequency variation. (B) Longitudinal displacement efficiency, S wave. (C) Energy efficiency, P wave. (D) Longitudinal Displacement efficiency, P wave. Note that fitted curves coincide in (C) and (D) due limited degrees of freedom in the harmonic oscillator model of equation (18).

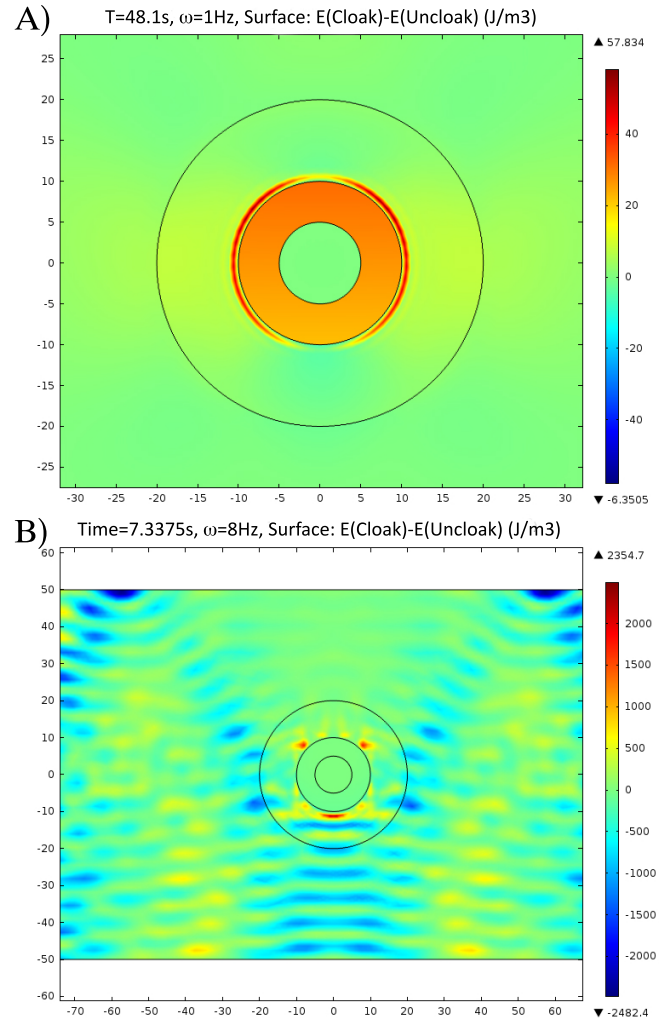


FIG. 3: Time domain simulations of SEC for VI S waves. Surface plot is energy difference $E_C - E_U$, i.e. positive values (reds) denote lower efficiency and negative values (blues) denote higher efficiency. Field generated by post-processing the displacement field $u(x, t)$ from dynamical simulations in COMSOL. Simulations were paired, with E_C and E_U generated from different instantiations using identical boundary and initial conditions but with the SEC present or absent respectively. This allowed for the generation of the scattered energy field without any explicit scattering field methodology. (A) Simulation at resonance, $\omega = 1\text{Hz}$. Note buildup of energy within the concrete tunnel (inner annulus) and the surface wave surrounding it. (B) Simulation above resonance, $\omega = 8\text{Hz}$. Note the surface wave is localized and does not surround the tunnel. View is zoomed out compared to (A) to display scattering field variation.

field surrounds the interior domain. Since the elastic wave equations depend upon a Laplacian, they obey the mean value theorem, implying that such a uniform energy buildup is able to penetrate through any cloak, even a perfect one [43–46].

However, for a perfect cloak, the penetration would merely imply $\eta = 0$, the presence of a negative efficiency implies that our SEC is still underperforming. In particular, a perfect cloak would not produce the energy buildup that we ob-

served in Figure 3. As has been observed in other approximate cloaks [19, 22, 35], imperfections can induce resonant modes within the cloak. If we assume that the observed surface modes are resonantly excited by the SEC, we can predict a simple model for how the cloak should effect the response, using the standard 1D simple harmonic oscillator (SHO) dynamical response

$$u = \frac{F/m}{\sqrt{(\omega^2 - \omega_c^2)^2 + \omega^2 \Gamma^2}} \quad (17)$$

where F/m is the effective acceleration and Γ is the damping rate. This would predict an efficiency of

$$\eta^{SHO}(\Omega, Q) = 1 - \frac{1}{\sqrt{(\Omega^2 - 1)^2 + \Omega^2/4Q^2}} \quad (18)$$

where $\Omega = \omega/\omega_c$ is the dimensionless frequency and $Q = \omega_c/2\Gamma$ is the resonator quality factor. This predicts an efficiency of 0 for $\Omega = 0, 2 - 1/4Q^2$, a minimum of $\eta = 1 - 2Q$ for $\Omega = 1$, and $\eta \rightarrow 1$ for $\Omega \rightarrow \infty$, which is qualitatively similar to our calculated efficiencies for $\eta(E)$ (see solid curves in Figure 2). For comparison, a perfect cloak efficiency should resemble a step function, jumping from 0 to 1 at $\Omega = 1$.

While this harmonic oscillator model predicts the qualitative aspects of the SEC's performance, the exact value of ω_c is not captured by that model. Since that determines the low frequency cutoff where the SEC's performance dramatically worsens, ω_c is critical to determining where the SEC is applicable and how it could be improved. If we substitute the equations (9) and (14) into equation (4) and apply some simple mathematical operations (see supplement), we can derive an implicit series solution for u . Notably, this implicit solution possesses a set of dimensionless parameters

$$\omega^2 a^2 \left(\frac{b}{b-a} \right)^2 \frac{1}{v_i^2}. \quad (19)$$

Plugging in the parameters used in our simulations gives $\omega_{c,S} = 0.9286\text{Hz}$ and $\omega_{c,P} = 2.275\text{Hz}$, which closely match our numerical results. Notice too that

$$\omega_{c,i} = \frac{b-a}{b} v_i \frac{1}{a}, \quad (20)$$

which is equivalent to a wave with velocity $v_i(b-a)/b$ and wavelength $2\pi a$, i.e. a surface wave with wavelength equal to the circumference of the cloaked region. Importantly, equation (20) implies that $\omega_c \propto 1/a$, so increasing the size of the cloaked domain will lower the cutoff frequency. To calculate Q from first principles is a less trivial problem, so instead we treat it as a fitting parameter in our model and fit the efficiency characteristics of our SEC to get $\langle Q_S \rangle = 1.57$, $\langle Q_P \rangle = 3.89$. In principle, for a real SEC, its performance could be measured by finding the resonant frequency and performance of the SEC at that frequency. However, since no real material possesses the inhomogeneities of equations (9), (14), a real SEC would likely be constructed from constituent elements

that approximate this (as in the standard cloak design [15]). As such, it should possess an upper cutoff frequency with wavelength of approximately the size of constituent element. We therefore expect an SEC to be effective for blocking frequencies between $\omega_c \propto 1/a < \omega < \omega_{MM} \propto 1/L$, where ω_{MM} is the characteristic frequency for a metamaterial of characteristic length L . The design of seismic metamaterials is a relatively new field [47–49] but shows a great deal of progress, and when combined with techniques like additive manufacturing [50] it suggests the feasibility of realizing an SEC. Additionally, while the coordinate transformation used here necessitates the engineering of both stiffness and the density of the metamaterials, more complicated transformations exist that simplify the material requirements. In particular, Ref. [51] would result in a design that only required engineering the elasticity and would leave the density unchanged (i.e. uniformly equal to the surrounding medium's density).

To determine the impact of this upper frequency cutoff and the feasibility of the SEC under more realistic conditions, we repeat our calculations using a discretized SEC. As is the standard procedure in cloaking, we replace our inhomogeneous SEC given by equations (9) and (14) with a series of annular rings. Each ring's density and elasticity tensor are selected to be the average value of these equations in their respective region. In particular, we use 10 rings, each 1 meter thick, of uniform orthotropic material given by the mean value of the SEC in their 1 meter shells. Although one meter is still quite thick, a thinner discretization scheme was avoided to ensure that the effects of discretization weren't disguised by an unrealistic number of layers and that the size of the rings was not significantly finer than the mesh grid used in our finite element simulations. On the other hand, even a single layer would be too thin to display the predicted cutoff due to wave scattering on the discretized structure. A 10 meter thick shell (i.e. a uniform layer of thickness equal to our SEC) would have an upper cutoff frequency of approximately 73 Hz, far above the 10 Hz practical limit that we employ (a shell engineered to be thin enough to be practical, then, would likely have an upper cutoff frequency in the $O(100)$ Hz range). In this regime, then, we expect that the principle limitation to the discretized SEC's performance is not the geometric effect of the shell thickness but simply the deviation of the material properties from continuous limit. As 10 layers typically shows good agreement with the continuous limit in experimental tests of metamaterial cloaks, we thus consider this case as the rigorous practical test of a realizable SEC. Given the uniformity of the continuous SEC's performance under different angles of incidence, polarizations, and efficiency measures, we focus on the energy shielding of the discretized SEC for bulk S and P waves under vertical incidence. We find in Fig. 4 that the behavior is in good agreement with the continuous SEC case, even as the discretization removes the singular behavior of the cloak at the inner boundary. In particular, we find clear agreement in the location of the lower cutoff frequency, qualitative wave dynamics, quantitative trend, and maximum efficiency. Moreover, we do not observe any decrease in performance due to

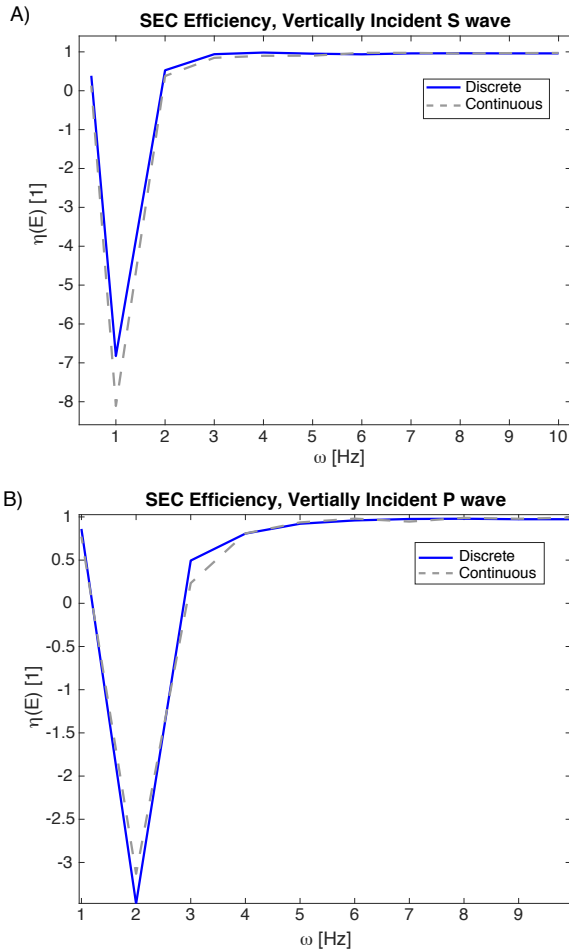


FIG. 4: Comparison of efficiency for the continuous (dotted grey line) and discrete (solid blue line) implementation of the SEC as a function of frequency. All plots are for vertical incidence. (A) Energy efficiency, S wave. (B) Energy efficiency, P wave.

the discretization, even at high frequencies, as the frequency range of interest is far lower than the upper cutoff frequency. We thus conclude that an SEC made from ordinary orthotropic material with tuned properties is an effective VIEE structure with much less limiting fabrication constraints.

To summarize, we have developed a method of modulating the challenge to realize asymmetries of a perfect elastic wave cloak into a more readily realized symmetric elastic cloak. By testing the performance of the cloak as a shield against seismic waves in a tunnel, we have demonstrated the feasibility of this design for VIEE, reducing the displacement within the cloaked tunnel by an order of magnitude for most of the frequencies corresponding to common seismic wave resonances (1-10Hz, [42]) (compared to a tunnel with no cloak). Since the frequency range where our approximate SEC fails is determined by the size of the cloaked region and the characteristic length of the SEC, switching to shield even larger regions ($a \gtrsim 100\text{m}$) and using sufficiently small building blocks for the SEC ($L \lesssim 1\text{m}$) should render this design quite effective for

blocking seismic waves of any relevant frequency for a large structure.

Alternatively, a smaller SEC could be used specifically to focus upon protecting equipment and critical infrastructure against high frequency elastic waves (5-20+ Hz). While these high frequency waves are often considered negligible in earthquake engineering due to their stronger dissipation, they can be dangerous in certain situations such as the survival of control equipment and circuits. Geological conditions can lead to larger content of higher frequencies [52]. Smaller structures can have their own higher resonant frequencies as well. Since this can include internal resonances of walls, excitation of strong ground motion in soil, or the failure of critical infrastructure like water pipes, generators, etc. [42, 53], the potential impact of high frequency waves can be immense and catastrophic. Furthermore, as the failure modes of the SEC are focused around a critical frequency corresponding to surface elastic waves on the inner boundary of the SEC, the inclusion of damping or resonance shifting techniques practices in VIEE [1] could be used to create a hybrid SEC/traditional earthquake abatement system with improved performance. Moreover, as cloak designs have been developed for various geometries [13–16] and could in principle be adapted to arbitrary geometric configurations, it is likely that this SEC approach could find ready application in a variety of critical structures.

ACKNOWLEDGEMENTS

We would like to thank Prof. Kathryn Matlack and Prof. Fatemeh Pourahmadian for their helpful discussion and suggestions.

SUPPLEMENTARY MATERIALS

Velocity and Acceleration Performance

The SEC's efficiency for shielding against velocity or acceleration transmission closely matches its efficiency for shielding against displacement. This makes intuitive sense, as these quantities are expected to differ by factors of ω , which cancel when we take the ratio of cloaked and uncloaked fields to calculate the efficiency.

Transverse Component Efficiency

While the overall trends for the efficiencies of the SEC for transverse components are similar to the longitudinal response of the main text, some deviations exist. However, these can be explained as arising from the relative magnitudes of the transverse and longitudinal components of the scattered waves, as only a tiny portion of the energy is relegated to these transverse modes, small fluctuations or numerical artifacts can

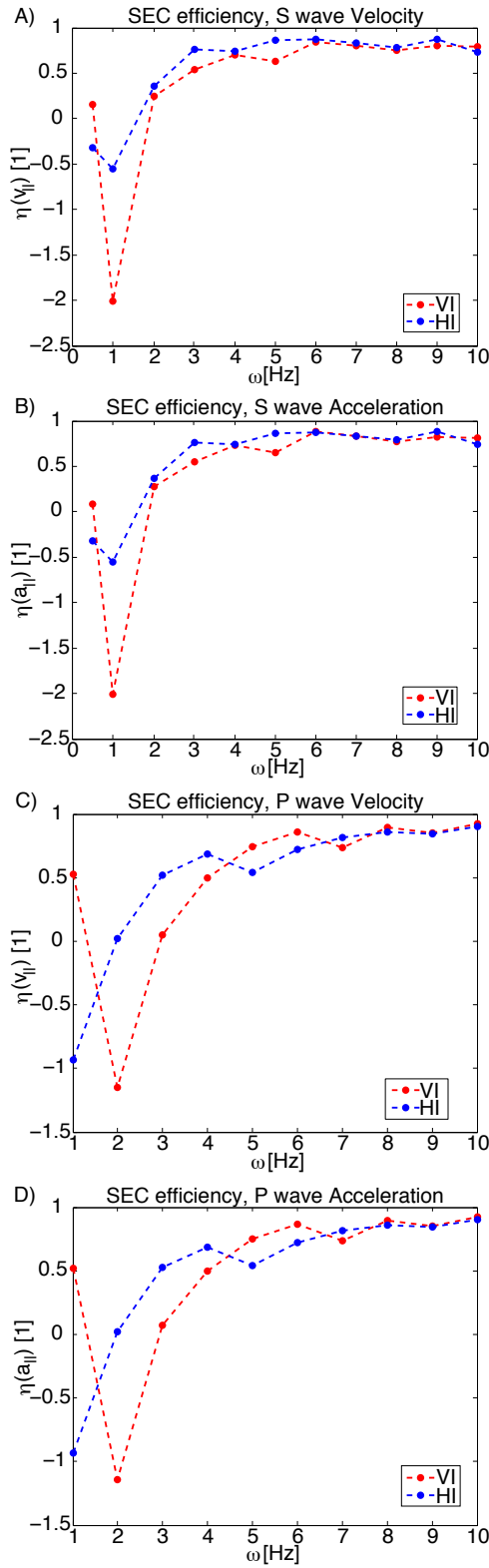


FIG. 5: Longitudinal component efficiency plots for the SEC as a function of frequency. Red dashed curve is data for vertical incidence (VI, wave from beneath the SEC), blue dashed curve is data for horizontal incidence (HI, wave from the left side of the SEC). (A) Velocity efficiency, S wave. (B) Acceleration efficiency, S wave. (C) Velocity efficiency, P wave. (D) Acceleration efficiency, P wave.

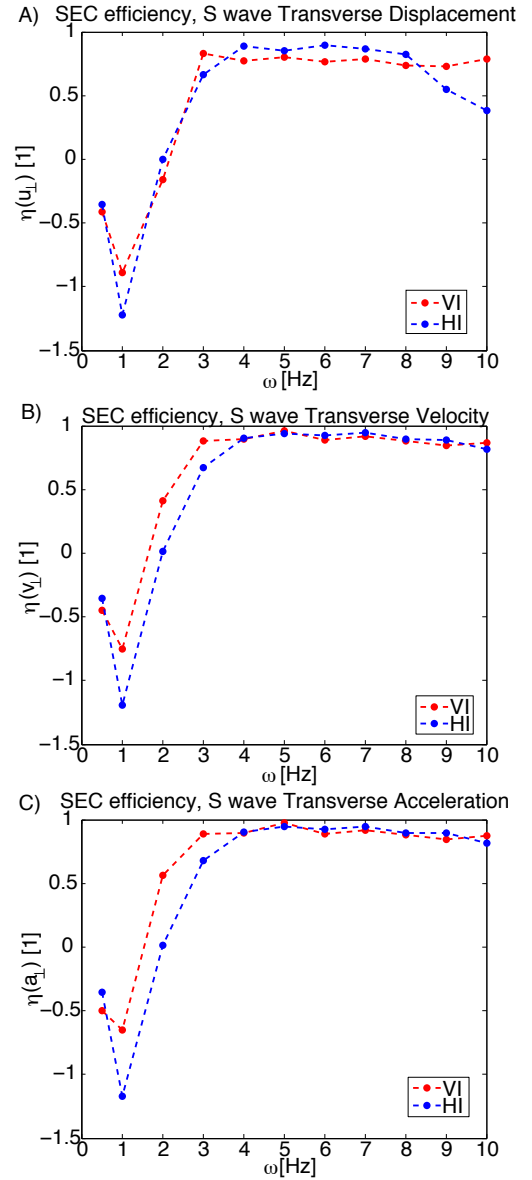


FIG. 6: Transverse component, S wave efficiency plots for the SEC as a function of frequency. Red dashed curve is data for vertical incidence (VI, wave from beneath the SEC), blue dashed curve is data for horizontal incidence (HI, wave from the left side of the SEC). (A) Displacement, (B) Velocity, (C) Acceleration.

have a large impact upon the calculated efficiency. Thus, these deviations from the longitudinal response are likely insignificant.

Dimensionless Constants

To find the dimensionless constants of the SEC we plug the parameters of equations (9) and (14) into equation (4). We assume that variation along z is negligible and thus specialize to polar coordinates, assuming a solution to the equations of

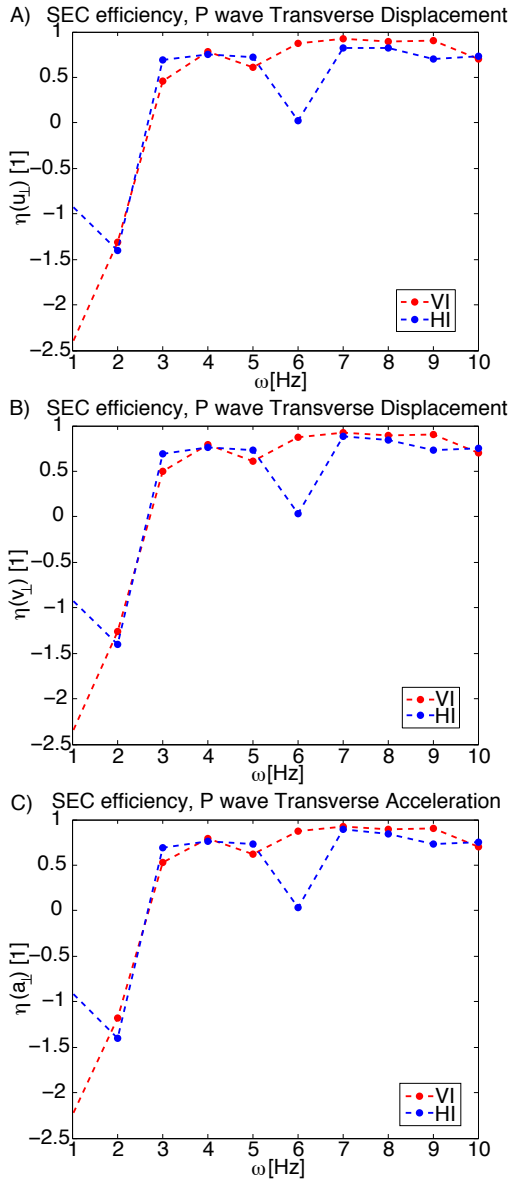


FIG. 7: Transverse component, P wave efficiency plots for the SEC as a function of frequency. Red dashed curve is data for vertical incidence (VI, wave from beneath the SEC), blue dashed curve is data for horizontal incidence (HI, wave from the left side of the SEC). (A) Displacement, (B) Velocity, (C) Acceleration.

motion

$$\vec{u} = \left(R_r(r)\hat{r} + R_\theta(r)\hat{\theta} \right) e^{i\omega t + in\theta} \quad (21)$$

where ω, n are the temporal and azimuthal eigenvalues under separation of variables. Plugging these in and multiplying the

equations of motion by $r(r-a)$ gives

$$\begin{aligned} -\omega^2(r-a)^2\left(\frac{b}{b-a}\right)^2\frac{\rho}{\lambda+2\mu}R_r &= (r-a)^2R_r'' \\ &+ (r-a)R_r' - R_r - \left(1-\frac{a}{r}\right)n^2\frac{\mu}{\lambda+2\mu}R_r \\ &+ in\left(\frac{\lambda+\mu}{\lambda+2\mu}(r-a)R_\theta' - R_\theta - \frac{\mu}{\lambda+2\mu}\left(1-\frac{a}{r}\right)R_\theta\right) \end{aligned} \quad (22)$$

and

$$\begin{aligned} -\omega^2(r-a)^2\left(\frac{b}{b-a}\right)^2\frac{\rho}{\mu}R_\theta &= r(r-a)R_\theta'' \\ &+ (r-a)R_\theta' - \left(1-\frac{a}{r}\right)R_\theta - n^2\frac{\lambda+2\mu}{\mu}R_\theta \\ &+ in\left(\frac{\lambda+\mu}{\mu}(r-a)R_r' + \frac{\lambda+2\mu}{\mu}R_r + \left(1-\frac{a}{r}\right)R_r\right) \end{aligned} \quad (23)$$

which can be solved by the method of Frobenius for R_r, R_θ . Notably, though, the only terms which are independent of r or d/dr possess dimensionless parameters which can be used to define the scale of different variables. Some of these (e.g. $n^2\mu/(\lambda+2\mu)$) express obvious relations (e.g. the ratio of the speeds of sound times n^2), but

$$\xi_i = \omega^2 a^2 \left(\frac{b}{b-a}\right)^2 \frac{1}{v_i^2} \quad (24)$$

relates the frequency of the incoming waves to the natural length scale of the cloak and is thus a non-trivial parameter for this problem.

-
- [1] Mead, D.J., *Passive vibration isolation* (Wiley, Chichester, 1998).
 - [2] Chopra, A.K., *Dynamics of Structures, 3rd Edition* (Pearson, 2007).
 - [3] Reitherman, R.K., *Earthquakes and Engineers: An International History* (ASCE Press, Reston 2012).
 - [4] Towhata, I., *Geotechnical Earthquake Engineering* (Springer, Berlin, 2008).
 - [5] Br l e, S., Javelaud, E.H., Enoch, S. and Guenneau, S., Experiments on seismic metamaterials: Molding surface waves. *Phys. Rev. Lett.* **112**(13), 133901 (2014).
 - [6] Yan, Y., Laskar, A., Cheng, Z., Menq, F., Tang, Y., Mo, Y.L. and Shi, Z., Seismic isolation of two dimensional periodic foundations. *J. Appl. Phys.* **116**(4), 044908 (2014).
 - [7] Kr del, S., Thom , N., and Daraio, C., Wide band-gap seismic metastructures. *Extr. Mech. Lett.* **4**, 111 (2015).
 - [8] Yan, Y., Cheng, Z., Menq, F., Mo, Y.L., Tang, Y. and Shi, Z., Three dimensional periodic foundations for base seismic isolation. *Smart Mater. Struct.* **24**(7), 075006 (2015).
 - [9] Aravantinos-Zafiris, N. and Sigalas, M.M., Large scale phononic metamaterials for seismic isolation. *J. Appl. Phys.* **118**(6), 064901 (2015).
 - [10] Dertimanis, V.K., Antoniadis, I.A. and Chatzi, E.N., Feasibility analysis on the attenuation of strong ground motions using finite periodic lattices of mass-in-mass barriers. *J. Eng. Mech.* **142**(9), 04016060 (2016).

- [11] Palermo, A., Krödel, S., Marzani, A., and Daraio, C., Engineered metabarrier as shield from seismic surface waves. *Sci. Rep.* **6**, 39356 (2016).
- [12] Perez-Campous, X., *A Comprehensive Study of the Radiated Seismic Energy* (Stanford University, 2002).
- [13] Pendry, J.B., Schurig, D. and Smith, D.R., Controlling electromagnetic fields. *Science* **312**(5781), 1780 (2006).
- [14] Leonhardt, U., Optical conformal mapping. *Science* **312**(5781), 1777 (2006).
- [15] Schurig, D., Mock, J.J., Justice, B.J., Cummer, S.A., Pendry, J.B., Starr, A.F. and Smith, D.R., Metamaterial electromagnetic cloak at microwave frequencies. *Science* **314**(5801), 977 (2006).
- [16] Li, J. and Pendry, J.B., Hiding under the carpet: a new strategy for cloaking. *Phys. Rev. Lett.* **101**(20), 203901 (2008).
- [17] Liu, R., Ji, C., Mock, J.J., Chin, J.Y., Cui, T.J. and Smith, D.R., Broadband ground-plane cloak. *Science* **323**(5912), 366 (2009).
- [18] Ma, H.F. and Cui, T.J., Three-dimensional broadband ground-plane cloak made of metamaterials. *Nat. Commun.* **1**, 21 (2010).
- [19] Zhou, X., Hu, G. and Lu, T., Elastic wave transparency of a solid sphere coated with metamaterials. *Phys. Rev. B* **77**(2), 024101 (2008).
- [20] Brun, M., Guenneau, S. and Movchan, A.B., Achieving control of in-plane elastic waves. *Appl. Phys. Lett.* **94**(6), 061903 (2009).
- [21] Kadic, M., Bückmann, T., Schittny, R., Gumbsch, P., and Wegener, M., Pentamode metamaterials with independently tailored bulk modulus and mass density. *Phys. Rev. Appl.* **2**(5), 054007 (2014).
- [22] Diatta, A. and Guenneau, S., Controlling solid elastic waves with spherical cloaks. *Appl. Phys. Lett.* **105**(2), 021901 (2014).
- [23] Diatta, A., Achaoui, Y., Brûlé, S., Enoch, S., and Guenneau, S., Control of Rayleigh-like waves in thick plate Willis metamaterials. *AIP Adv.* **6**(12), 121707 (2016).
- [24] Khlopotin, A., Olsson, P. and Larsson, F., Transformational cloaking from seismic surface waves by micropolar metamaterials with finite couple stiffness. *Wave Motion* **58**, 53 (2015).
- [25] Diatta, A. and Guenneau, S., Elastodynamic cloaking and field enhancement for soft spheres. *J. Phys. D Appl. Phys.* **49**(44), 445101 (2016).
- [26] Milton, G.W., Briane, M. and Willis, J.R., On cloaking for elasticity and physical equations with a transformation invariant form. *New J. Phys.* **8**(10), 248 (2006).
- [27] Norris, A.N. and Shuvalov, A.L., Elastic cloaking theory. *Wave Motion* **48**(6), 525 (2011).
- [28] Chang, Z., Hu, J., Hu, G., Tao, R. and Wang, Y., Controlling elastic waves with isotropic materials. *Appl. Phys. Lett.* **98**(12), 121904 (2011).
- [29] Hu, J., Chang, Z. and Hu, G., Approximate method for controlling solid elastic waves by transformation media. *Phys. Rev. B* **84**(20), 201101 (2011).
- [30] Norris, A.N. and Parnell, W.J., Hyperelastic cloaking theory: transformation elasticity with pre-stressed solids. *Proc. R. Soc. A* **468**(2146), 2881 (2012).
- [31] Chang, Z., Liu, X., Hu, G. and Hu, J., Transformation ray method: Controlling high frequency elastic waves (L). *J. Acoust. Soc. Am.* **132**(4), 2942 (2012).
- [32] Parnell, W.J., Norris, A.N. and Shearer, T., Employing pre-stress to generate finite cloaks for antiplane elastic waves. *Appl. Phys. Lett.* **100**(17), 171907 (2012).
- [33] Parnell, W.J., Nonlinear pre-stress for cloaking from antiplane elastic waves. *Proc. R. Soc. A* **468**(2138), 563 (2012).
- [34] Parnell, W.J. and Shearer, T., Antiplane elastic wave cloaking using metamaterials, homogenization and hyperelasticity. *Wave Motion* **50**(7), 1140 (2013).
- [35] Hu, G. and Liu, H., Nearly cloaking the elastic wave fields. *J. Math. Pure. Appl.* **104**(6), 1045 (2015).
- [36] Beveridge, A., Wheel, M., and Nash, D., The micropolar elastic behavior of model macroscopically heterogeneous materials. *Int. J. Solids Struct.* **50**(1), 246266 (2013).
- [37] Wheel, M., Frame, J., and Riches, P., Is smaller always stiffer? On size effects in supposedly generalised continua. *Int. J. Solids Struct.* **6768**, 8492 (2015).
- [38] Norris, A.N. and Parnell, W.J. Hyperelastic Cloaking theory. In: *A handbook of metamaterials and nanophotonics*. Editors: Maier, S., Shamonina, K., Guenneau, S., Hess, O., and Aizpurua, J. (World Scientific, 2017).
- [39] Diatta, A., Kadic, M., Wegener, M. and Guenneau, S., Scattering problems in elastodynamics. *Phys. Rev. B* **94**(10), 100105(R) (2016).
- [40] Bückmann, T., Kadic, M., Schittny, R. and Wegener, M., Mechanical cloak design by direct lattice transformation. *Proc. Natl. Acad. Sci. USA* **112**(16), 49304 (2015).
- [41] COMSOL AB, *COMSOL Multiphysics User's Guide, Version 4.3b* (Burlington, 2013).
- [42] Meyer, P.K., *The Impact of High Frequency/Low Energy Seismic Waves on Unreinforced Masonry*, MS Thesis, MIT (2006).
- [43] Greenleaf, A., Lassas, M., and Uhlmann, G., Anisotropic conductivities that cannot be detected by EIT. *Physiol. Meas.* **24**(2), 413 (2003).
- [44] Greenleaf, A., Lassas, M., and Uhlmann, G., On nonuniqueness for Calderón's inverse problem. *Math. Res. Lett.* **10**, 685 (2003).
- [45] Greenleaf, A., Kurylev, Y., Lassas, M. and Uhlmann, G., Invisibility and inverse problems. *B. Am. Math. Soc.* **46**(1), 55 (2009).
- [46] Sklan, S., Cloaking of the momentum in acoustic waves. *Phys. Rev. E* **81**(1), 016606 (2010).
- [47] Finocchio, G., Casablanca, O., Ricciardi, G., Alibrandi, U., Garesci, F., Chiappini, M. and Azzerboni, B., Seismic metamaterials based on isochronous mechanical oscillators. *Appl. Phys. Lett.* **104**(19), 191903 (2014).
- [48] Bückmann, T., Schittny, R., Thiel, M., Kadic, M., Milton, G.W. and Wegener, M., 2014. On three-dimensional dilational elastic metamaterials. *New J. Phys.* **16**(3), 033032 (2014).
- [49] Zhou, X. and Hu, G., Analytic model of elastic metamaterials with local resonances. *Phys. Rev. B* **79**(19), 195109 (2009).
- [50] Gosselin, C., Duballet, R., Roux, P., Gaudillère, N., Dirrenberger, J. and Morel, P., Large-scale 3D printing of ultra-high performance concrete: a new processing route for architects and builders. *Mater. Design* **100**, 102 (2016).
- [51] Zareei, A. and Alam, M.R., Cloaking in shallow-water waves via nonlinear medium transformation. *J. Fluid Mech.* **778**, 273 (2015).
- [52] Davis, P.M., Rubinstein, J.L., Liu, K.H., Gao, S.S. and Knopoff, L., Northridge earthquake damage caused by geologic focusing of seismic waves. *Science* **289**(5485), 1746 (2000).
- [53] Massarsch, K.R. and Fellenius, B.H., Deep vibratory compaction of granular soils. *Elsevier Geo-Engineering Book Series* **3**, 539 (2005).